

Neuropeptide Y regulates a vascular gateway for hematopoietic stem and progenitor cells

Pratibha Singh,¹ Jonathan Hoggatt,^{1,2} Malgorzata M. Kamocka,³ Khalid S. Mohammad,⁴ Mary R. Saunders,¹ Hongge Li,¹ Jennifer Speth,¹ Nadia Carlesso,^{5,6} Theresa A. Guise,⁴ and Louis M. Pelus¹

¹Department of Microbiology & Immunology, Indiana University School of Medicine, Indianapolis, Indiana, USA. ²Cancer Center and Center for Transplantation Sciences, Massachusetts General Hospital, Harvard Medical School, Boston, Massachusetts, USA. ³Department of Medicine/Nephrology-ICBM Imaging Facility, ⁴Department of Medicine/Endocrinology, and ⁵Department of Pediatrics, Indiana University School of Medicine, Indianapolis, Indiana, USA. ⁶Department of Hematologic Malignancies Translational Science, Beckman Research Institute of City of Hope, Duarte, California, USA.

Endothelial cells (ECs) are components of the hematopoietic microenvironment and regulate hematopoietic stem and progenitor cell (HSPC) homeostasis. Cytokine treatments that cause HSPC trafficking to peripheral blood are associated with an increase in dipeptidylpeptidase 4/CD26 (DPP4/CD26), an enzyme that truncates the neurotransmitter neuropeptide Y (NPY). Here, we show that enzymatically altered NPY signaling in ECs caused reduced VE-cadherin and CD31 expression along EC junctions, resulting in increased vascular permeability and HSPC egress. Moreover, selective NPY2 and NPY5 receptor antagonists restored vascular integrity and limited HSPC mobilization, demonstrating that the enzymatically controlled vascular gateway specifically opens by cleavage of NPY by CD26 signaling via NPY2 and NPY5 receptors. Mice lacking CD26 or NPY exhibited impaired HSPC trafficking that was restored by treatment with truncated NPY. Thus, our results point to ECs as gatekeepers of HSPC trafficking and identify a CD26-mediated NPY axis that has potential as a pharmacologic target to regulate hematopoietic trafficking in homeostatic and stress conditions.

Introduction

Hematopoietic stem and progenitor cells (HSPCs) reside in bone marrow (BM) niches associated with supporting cells that regulate quiescence and proliferative fate decisions (1-3). At homeostasis, only a small pool of these cells circulates in the peripheral blood (PB), but this can be enhanced by a demand for accelerated hematopoiesis, e.g., in inflammation or bacterial sepsis or in response to immunological stress. Clinically, effective and robust HSPC trafficking is essential for both acquisition of HSPCs for transplantation and subsequent homing back to the recipient BM. Enforced egress of HSPCs to the circulation, a process termed mobilization, is widely used to acquire hematopoietic grafts for life-saving transplantation (4). Granulocyte colony-stimulating factor (G-CSF) is the primary agent used clinically to mobilize HSPCs and serves as an archetype for mechanistic insight into stem cell trafficking.

To better understand the physiologic regulators of HSPC trafficking with an aim toward improved therapies, we used G-CSF mobilization as a model system. Specifically, we were interested in understanding the mechanisms governing suboptimal HSPC trafficking after G-CSF treatment. Early studies identified a requirement for dipeptidyl peptidase 4/CD26 (DPP4/CD26) in the optimal HSPC mobilization response to G-CSF (5, 6), as either *Cd26* gene deletion or pharmacologic inhibition of DPP4 enzyme

activity significantly reduced HSPC mobilization. CD26 is a serine exopeptidase that cleaves N-terminal dipeptides when either alanine or proline is in the penultimate position. This enzymatic cleavage regulates the activity of numerous molecules including growth factors, chemokines, neuropeptides, and vasoactive peptides (7-11). Since CD26 can cleave and inactivate the chemokine SDF-1 *in vitro* (8, 12) and reduced BM SDF-1 is a hallmark found following G-CSF administration (13-15), CD26 cleavage of SDF-1 has been hypothesized to mediate G-CSF-directed HSPC egress. However, to date, evidence showing a direct association between CD26 and disruption of SDF-1 signaling *in vivo* during G-CSF administration has not been reported.

Surprisingly, we found that CD26 regulation of HSPC trafficking is independent of SDF-1 and, instead, identified a nonparadigmatic mechanism governing vascular permeability mediated by CD26-dependent cleavage of the neurotransmitter neuropeptide Y (NPY). Our findings identify a role for NPY in regulating vascular permeability and HSPC trafficking and describe what to our knowledge is a previously unrecognized active role of sinusoidal endothelial cells (SECs) as gatekeepers for HSPC egress from the marrow niche. These results also define a potential pharmaceutical target on vascular ECs to regulate barrier integrity for a variety of immunologic stressors.

Results

HSPC-intrinsic CD26 expression is not required for BM egress. The CD26 cell-surface protease has been shown to affect HSPC trafficking and function. Pharmacologic inhibition of CD26 enzyme activity or *Cd26* gene deletion in mice was shown to reduce HSPC egress from BM in response to G-CSF (5, 6). This reduction in

► Related Commentary: p. 4231

Conflict of interest: The authors have declared that no conflict of interest exists.

Submitted: April 20, 2017; **Accepted:** September 12, 2017.

Reference information: *J Clin Invest.* 2017;127(12):4527-4540.

<https://doi.org/10.1172/JCI94687>

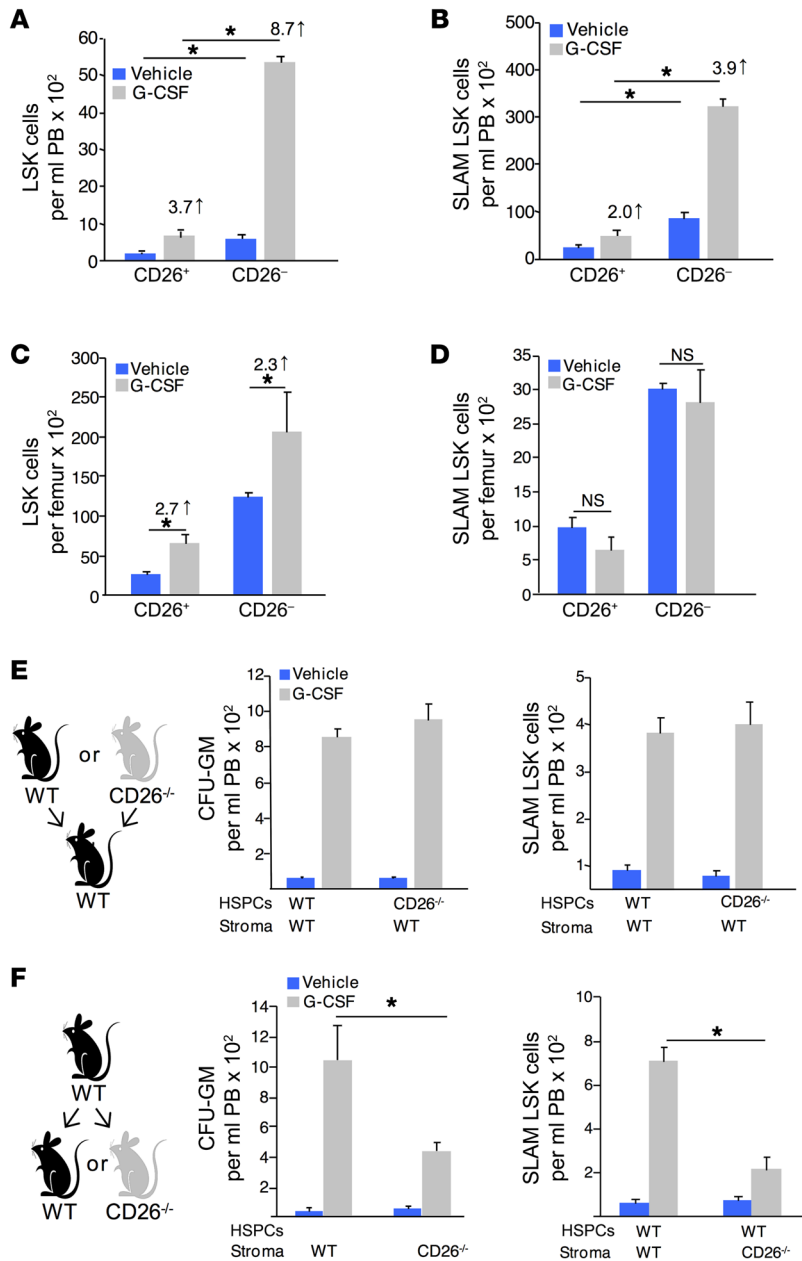


Figure 1. CD26 expressed by stromal cells, but not HSPCs, regulates HSPC trafficking. CD26 expression on PB LSK (A) and SLAM LSK (B) cells (mean ± SEM; $n = 3$ mice/group/experiment, each assayed individually; $n = 3$ experiments). CD26 expression on BM LSK (C) and SLAM LSK (D) cells (mean ± SEM/femur; 1 of 2 independent experiments; $n = 4$ mice/group/experiment, each assayed individually). (E and F) HSPC mobilization in chimeric mice. (E) CD26^{-/-} donor cells transplanted into WT recipients and (F) WT donor cells transplanted into CD26^{-/-} recipients. Two months after transplantation, mice were treated with G-CSF, and PB hematopoietic progenitor cells (HPCs) were determined by CFC assay, and SLAM LSK cells were analyzed by flow cytometry (mean ± SEM; $n \geq 5$ mice/group, each assayed individually). * $P \leq 0.05$, by 1-way ANOVA with Sidak's multiple comparisons test.

itor cell content in PB after G-CSF administration was significantly lower in the absence or inhibition of CD26 activity (Supplemental Figure 1A; supplemental material available online with this article; <https://doi.org/10.1172/JCI94687DS1>). In addition, we detected reduced numbers of hematopoietic stem cells (HSCs) (CD150⁺ [SLAM] CD48⁻ signaling lymphocytic activation molecule Lin⁻SCA1⁺c-Kit⁺ [LSK] cells) in PB (Supplemental Figure 1B). We further extended these findings by showing that fewer long-term repopulating HSCs were mobilized when CD26 activity was inhibited, comparing PB grafts from mice treated with G-CSF or G-CSF plus diproton A (Supplemental Figure 1C).

When mobilized HSPCs were evaluated for CD26 expression, we unexpectedly observed that most mobilized LSK (Figure 1A) and SLAM LSK (Figure 1B) cells were CD26⁻, suggesting that intrinsic CD26 expression was not required for their mobilization. Reduced egress of CD26-expressing HSPCs following G-CSF treatment did not result from impaired expansion or differentiation, since the proportion of marrow LSK cells expressing CD26 at baseline and after G-CSF treatment increased to an equivalent degree (Figure 1C), and no change in total SLAM LSK cells or the proportion of cells expressing CD26 was observed following G-CSF administration (Figure 1D). In addition,

we found that CD26 expression on LSK and SLAM LSK cells was not altered by G-CSF treatment (Supplemental Figure 1D). To further investigate the role of intrinsic versus extrinsic CD26, we created chimeric mice by transplanting BM cells from WT or CD26^{-/-} mice into syngeneic WT or CD26^{-/-} recipient mice. WT recipients transplanted with WT or CD26^{-/-} cells showed normal HSPC mobilization after G-CSF administration (Figure 1E). However, CD26^{-/-} recipient mice transplanted with WT hematopoietic cells showed attenuated mobilization in response to G-CSF (Figure 1F). These data indicate that CD26 expression on stromal, rather than hematopoietic, cells is required for optimal HSPC trafficking.

When mobilized HSPCs were evaluated for CD26 expression, we unexpectedly observed that most mobilized LSK (Figure 1A) and SLAM LSK (Figure 1B) cells were CD26⁻, suggesting that intrinsic CD26 expression was not required for their mobilization.

Reduced egress of CD26-expressing HSPCs following G-CSF treatment did not result from impaired expansion or differentiation, since the proportion of marrow LSK cells expressing CD26 at baseline and after G-CSF treatment increased to an equivalent degree (Figure 1C), and no change in total SLAM LSK cells or the proportion of cells expressing CD26 was observed following G-CSF administration (Figure 1D). In addition,

we found that CD26 expression on LSK and SLAM LSK cells was not altered by G-CSF treatment (Supplemental Figure 1D). To further investigate the role of intrinsic versus extrinsic CD26, we created chimeric mice by transplanting BM cells from WT or CD26^{-/-} mice into syngeneic WT or CD26^{-/-} recipient mice. WT recipients transplanted with WT or CD26^{-/-} cells showed normal HSPC mobilization after G-CSF administration (Figure 1E). However, CD26^{-/-} recipient mice transplanted with WT hematopoietic cells showed attenuated mobilization in response to G-CSF (Figure 1F). These data indicate that CD26 expression on stromal, rather than hematopoietic, cells is required for optimal HSPC trafficking.

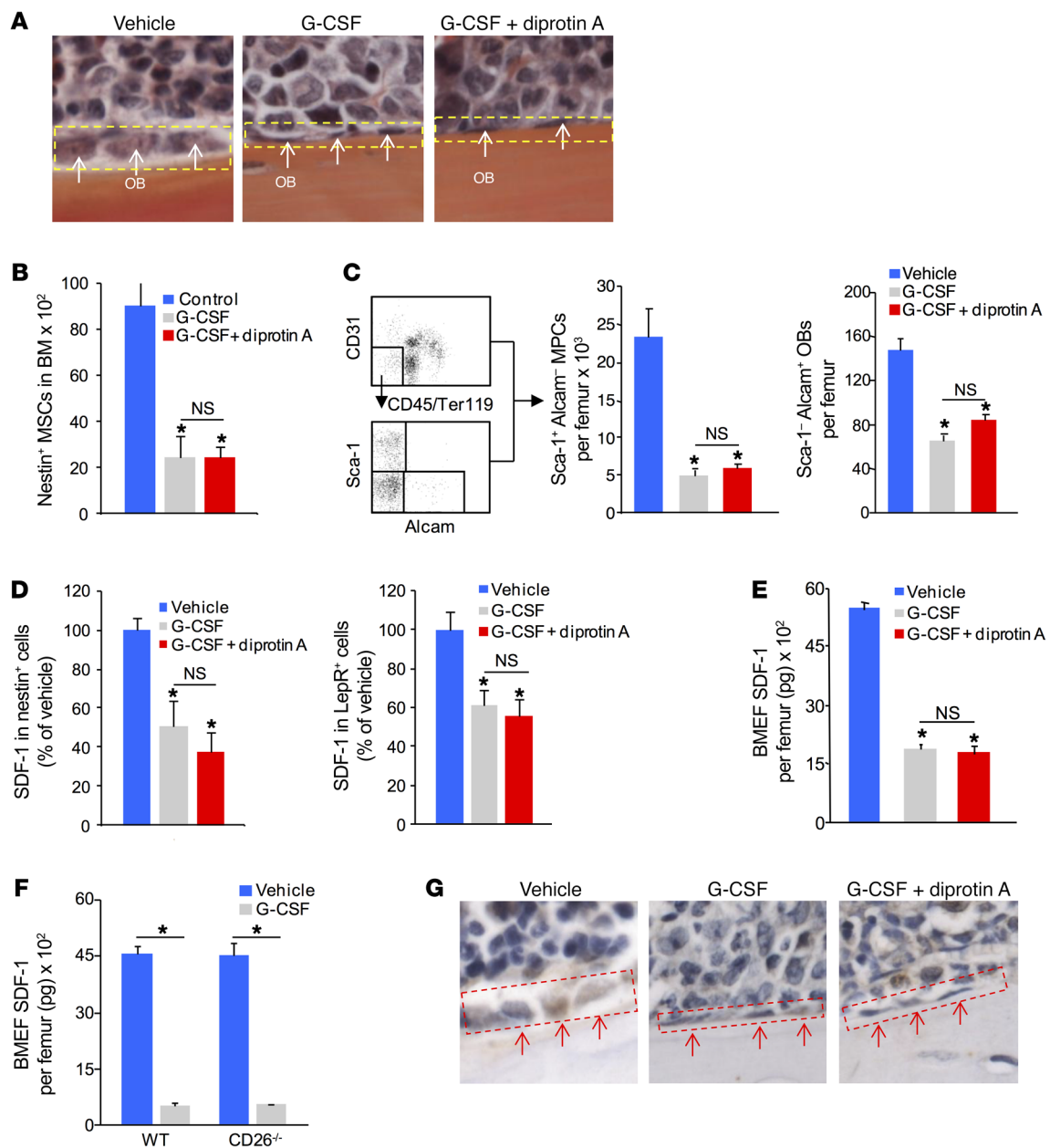


Figure 2. Suppression of niche components in response to G-CSF administration is independent of CD26 activity. (A) Representative histology of endosteal lining osteolineage cells in G-CSF⁻ and G-CSF plus diprotin A-treated mice (original magnification, ×400). (B and C) MSCs, MPCs, and OBs in BM from mice treated with G-CSF or G-CSF plus diprotin A. (B) MSCs (CD45⁻CD31⁺nestin⁺) and (C) MPCs (CD45⁻Sca-1⁺Alcam⁻) and OBs (CD45⁻Sca-1⁺Alcam⁺) (mean ± SEM; *n* = 5 mice/group). (D) SDF-1 expression in BM nestin⁺ MSCs and leptin receptor⁺ (LepR⁺) cells. (E) SDF-1 levels in BMEF from WT mice treated with G-CSF or G-CSF plus diprotin A and from (F) CD26^{-/-} mice treated with G-CSF. SDF-1 was measured by ELISA (mean ± SEM; *n* ≥ 5 mice/group). (G) Immunohistochemical staining of SDF-1 after treatment of mice with G-CSF or G-CSF plus diprotin A (original magnification, ×400). The red-outlined areas are endosteal lining and arrows indicate SDF-1 positive osteolineage cells. **P* ≤ 0.05 compared with vehicle, by 1-way ANOVA with Sidak's multiple comparisons test.

mouse chimera study indicated a requirement for stromal CD26 for optimal mobilization to G-CSF, we explored whether MSPC and osteolineage cell numbers and/or function were altered in the absence of CD26 activity. As previously described, osteoblast (OB) laminarity/flattening increases after G-CSF treatment, however, blockade of CD26 activity did not alter this response (Figure 2A). Total numbers of nestin⁺ mesenchymal stem cells (MSCs) (17), CD45⁻CD119⁻CD31⁺Sca-1⁺Alcam⁻ cells enriched for mesenchymal progenitor cells (MPCs), and CD45⁻CD119⁻CD31⁺Sca-

1⁺Alcam⁺ cells enriched for OBs (20) were reduced equivalently in mice treated with G-CSF or G-CSF plus diprotin A (Figure 2, B and C). SDF-1 protein expression in nestin⁺ MSCs and leptin receptor⁺ mesenchymal stromal cells (21) was also reduced to the same degree, with or without diprotin A (Figure 2D and Supplemental Figure 2A). Similarly, total SDF-1 protein levels in BM were reduced to the same degree, with or without diprotin A (Figure 2E), and in CD26^{-/-} mice treated with G-CSF (Figure 2F). Immunohistochemical analysis showed similarly reduced SDF-1 in bone-

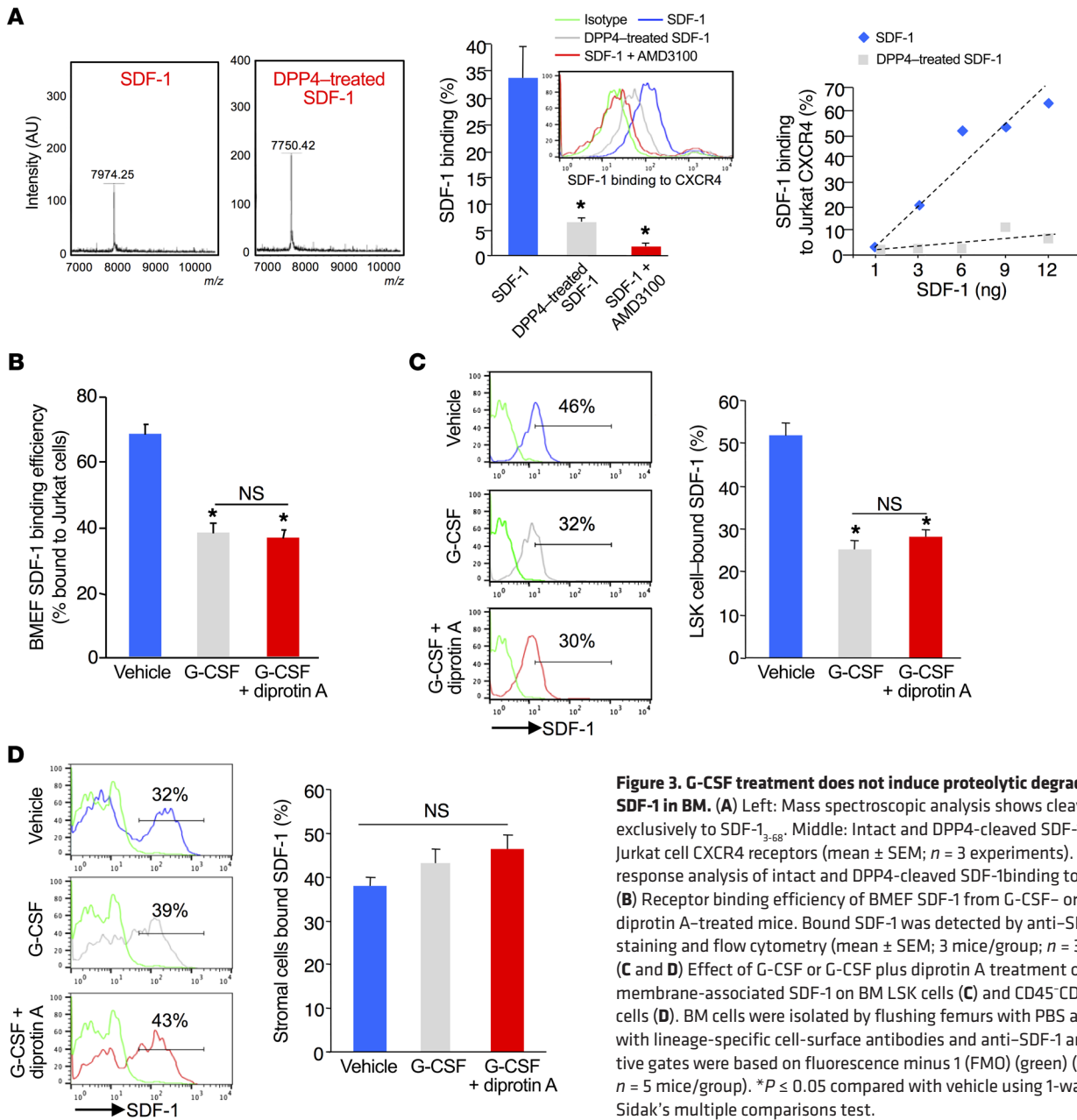


Figure 3. G-CSF treatment does not induce proteolytic degradation of SDF-1 in BM. (A) Left: Mass spectroscopic analysis shows cleavage of SDF-1 exclusively to SDF-1₃₋₆₈. Middle: Intact and DPP4-cleaved SDF-1 binding to Jurkat cell CXCR4 receptors (mean ± SEM; n = 3 experiments). Right: Dose response analysis of intact and DPP4-cleaved SDF-1 binding to Jurkat CXCR4. (B) Receptor binding efficiency of BMEF SDF-1 from G-CSF- or G-CSF plus diprotin A-treated mice. Bound SDF-1 was detected by anti-SDF-1 antibody staining and flow cytometry (mean ± SEM; 3 mice/group; n = 3 experiments). (C and D) Effect of G-CSF or G-CSF plus diprotin A treatment on levels of membrane-associated SDF-1 on BM LSK cells (C) and CD45⁺CD119⁻ stromal cells (D). BM cells were isolated by flushing femurs with PBS and stained with lineage-specific cell-surface antibodies and anti-SDF-1 antibody. Positive gates were based on fluorescence minus 1 (FMO) (green) (mean ± SEM; n = 5 mice/group). *P ≤ 0.05 compared with vehicle using 1-way ANOVA with Sidak's multiple comparisons test.

lining osteolineage cells in both treatment groups as well (Figure 2G). In addition, BM levels of the hematopoietic retention factors osteoprotegerin and SCF were not affected by inhibition of CD26 proteolytic activity (Supplemental Figure 2, B and C). We found that matrix metalloproteinase 9 (MMP-9) levels were increased equivalently in the BM of G-CSF- or G-CSF plus diprotin A-treated mice (Supplemental Figure 2D). CD26 expression was not altered on nestin⁺ MSCs following either treatment regimen (Supplemental Figure 2E). Moreover, CD26 proteolytic activity on the CD45⁺Ter119⁻CD31⁻ nonendothelial stromal cell population enriched for MSCs, osteolineage cells, and perivascular cells was unaffected by G-CSF (Supplemental Figure 2F). These results demonstrate that the decrease in G-CSF mobilization in the absence of CD26 activity is not due to differences in stromal niche attenuation or cytokines or factors associated with HSPC retention in BM.

G-CSF does not induce CD26-dependent degradation of SDF-1. Our chimeric mouse transplantation studies demonstrated a stromal requirement for CD26 regulation of HSPC trafficking, with no apparent changes in mesenchymal stromal or osteolineage cells or in the molecular players implicated in mobilization. The commonly accepted paradigm for reduced mobilization in the absence of CD26 activity is that intact BM SDF-1 maintains HSPC retention. We observed significant (Figure 2, E and F) and equivalent reductions of SDF-1 in the BM following G-CSF administration, regardless of the inhibition or absence of CD26. However, since ELISA cannot discriminate between full-length and cleaved SDF-1, the SDF-1 remaining in the BM in control mice after G-CSF treatment could represent cleaved inactive SDF-1, while in CD26^{-/-} mice, the SDF-1 detected was intact and could serve to retain HSPCs. To discriminate full-length and trun-

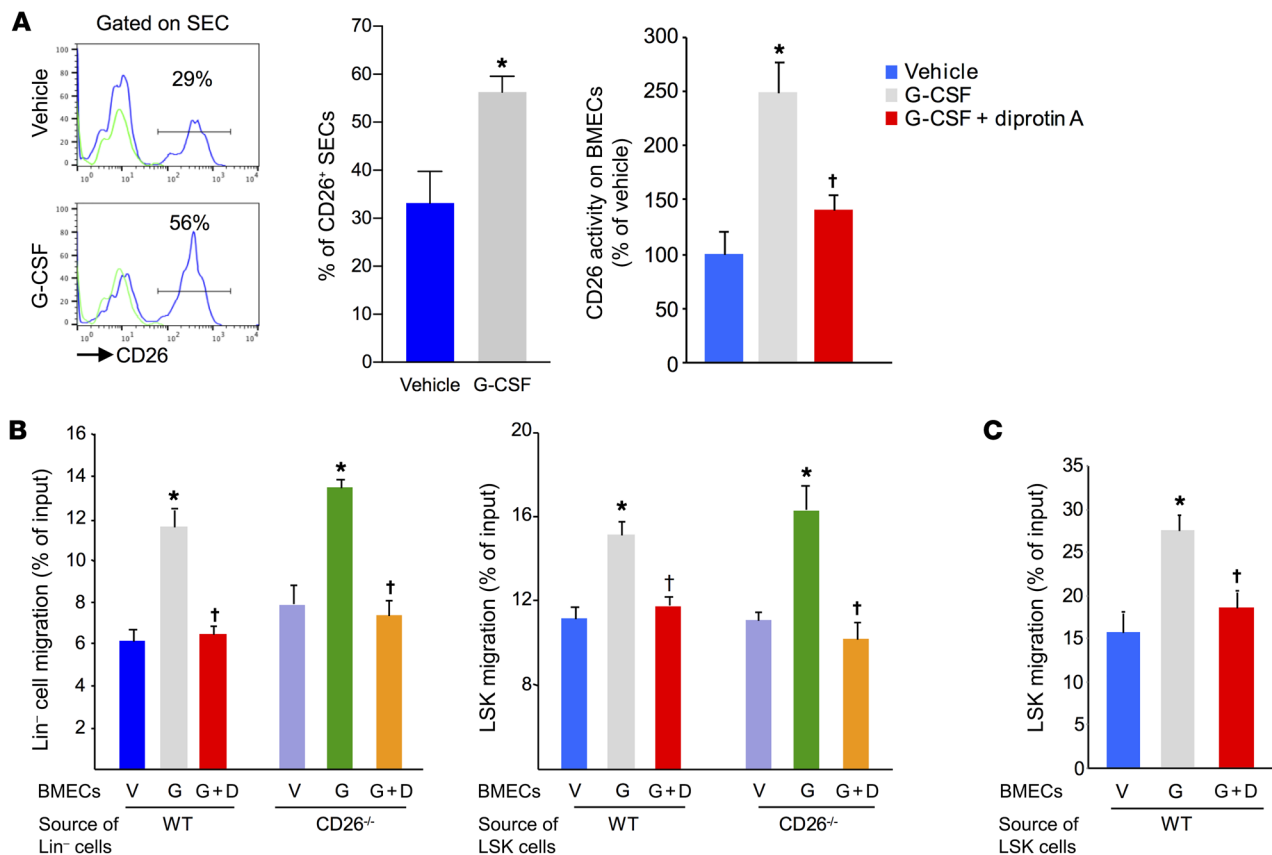


Figure 4. G-CSF treatment increases CD26 expression on BMECs and enhances transendothelial migration of HPCs. (A) CD26 expression (left and middle) and CD26 proteolytic activity (right) on BM SECs (CD45⁺Ter119⁺VEGFR3⁺VE-cadherin⁺CD31⁺) from mice treated with G-CSF or G-CSF plus diprotin A. Positive gates for CD26 expression were based on FMO (green) (mean \pm SEM, $n = 5$ mice/group). (B) Migration of WT and CD26^{-/-} Lin⁻ and LSK cells across G-CSF- or G-CSF plus diprotin A-treated BMEC monolayers to 100 ng/ml SDF-1 (mean \pm SEM; $n = 2$ experiments). (C) Transendothelial migration of LSK cells to 100 ng/ml S1P (mean \pm SEM; $n = 2$ experiments). * $P < 0.05$ compared with vehicle and † $P \leq 0.05$ compared with G-CSF, by Student's t test (A, left) or 1-way ANOVA with Sidak's multiple comparisons test (A, right, B and C). V, vehicle; G, G-CSF; G+D, G-CSF plus diprotin A.

cated SDF-1 in the BM, we quantitated SDF-1 binding to CXCR4 by flow cytometry, taking advantage of the fact that N-terminal-cleaved SDF-1₃₋₆₈ has a 10-fold reduction in its binding efficiency to its receptor CXCR4 (22). As reported, CD26 cleaved full-length SDF-1 to SDF-1₃₋₆₈ (Figure 3A, left), which reduced binding to Jurkat T cell CXCR4 (Figure 3A, middle). We confirmed the specificity of SDF-1 binding to Jurkat CXCR4 using the selective CXCR4 antagonist AMD3100 (Figure 3A, center). Dose response analysis showed that the Jurkat CXCR4 binding assay quantitated SDF-1 with high sensitivity (Figure 3A, right). When compared with vehicle-treated mice, samples of BM extracellular fluid (BMEF) from G-CSF-treated mice had significantly lower SDF-1 binding to CXCR4 (Figure 3B), consistent with the reduced SDF-1 protein levels measured by ELISA (Figure 2E). CD26 inhibition did not reverse G-CSF-mediated attenuation of SDF-1 binding, despite the fact that the mobilization of HSPCs was significantly reduced. Since HSPC retention in the BM is known to be more influenced by localized SDF-1 concentration than by soluble SDF-1, we measured membrane-bound SDF-1 levels on HSPCs and stromal cells. We found that LSK cell-surface-bound SDF-1 was substantially reduced following G-CSF administration and was not restored by inhibition of CD26 activity (Figure 3C). Stromal cell (CD45⁻

Ter119⁻) membrane-associated SDF-1 levels were also equivalent to those in vehicle control in the G-CSF and G-CSF-plus-diprotin A samples (Figure 3D). These data indicate that proteolytic degradation and inactivation of SDF-1 is not a primary mechanism through which CD26 affects mobilization by G-CSF.

G-CSF increases EC CD26 and enhances HSPC transendothelial migration. HSCs are found in perivascular regions proximal to SECs and reticular cells (23–25) and have recently been reported to be in contact with VE-cadherin⁺ cells (25). Mouse BM ECs (BMECs) (Supplemental Figure 3A), including SECs (Supplemental Figure 3B), express mRNA and protein for the G-CSF receptor. While exploring the marrow microenvironment after G-CSF treatment, we observed an increased frequency of CD26⁺CD45⁺Ter119⁺VEGFR3⁺VE-cadherin⁺CD31⁺ SECs (Figure 4A). We found that CD26 proteolytic activity was similarly increased and was effectively blocked by diprotin A (Figure 4A, right).

Since HSPCs must transmigrate across the endothelium to enter PB, and given that we observed a selective increase in CD26 on ECs after G-CSF administration, we hypothesized that perhaps EC CD26 regulates HSPC egress. To test this hypothesis, we first evaluated HSPC migration across monolayers of mouse BMECs in vitro as a model for HSPC egress. In the transmigration

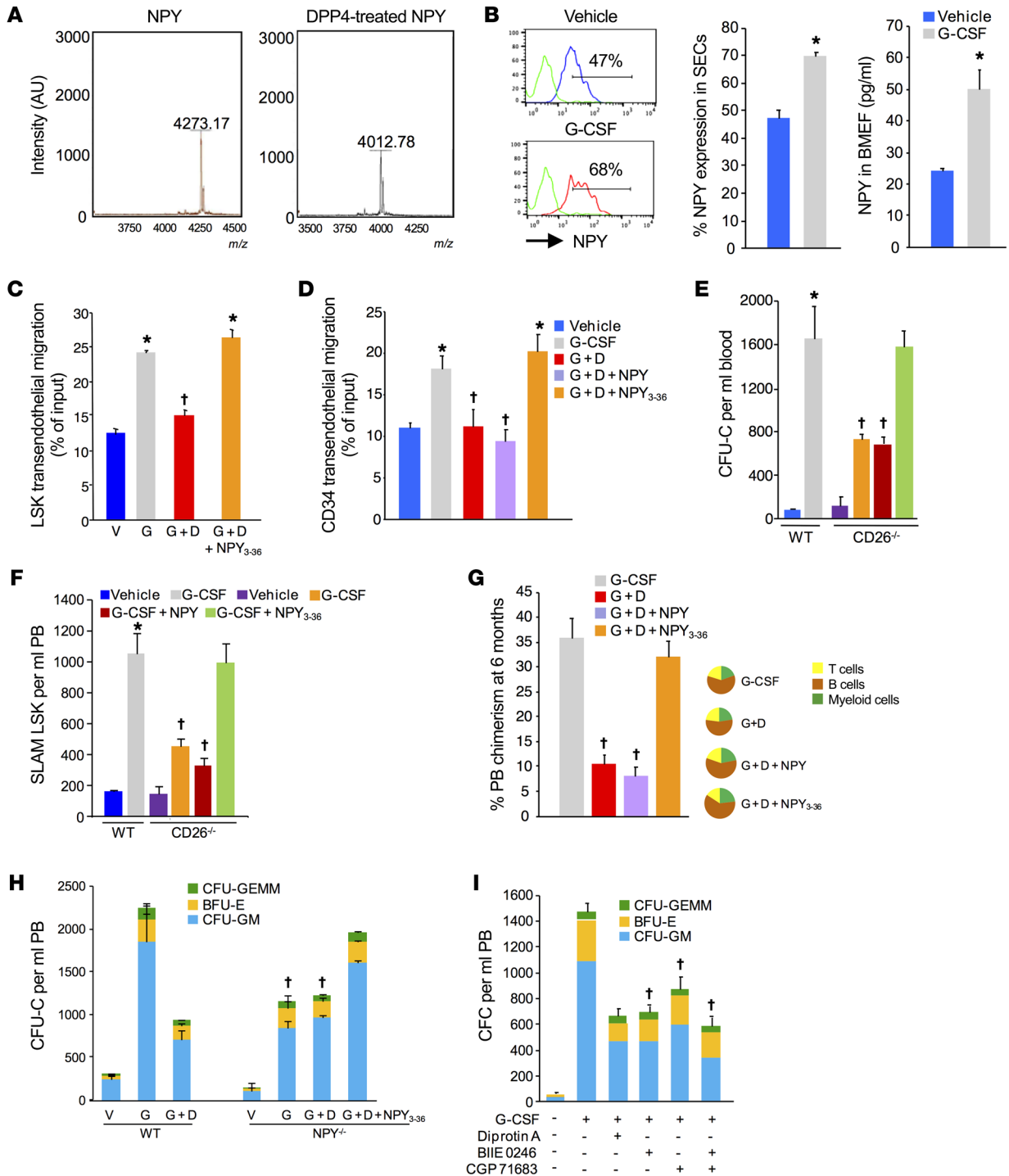


Figure 5. NPY₃₋₃₆ reverses the CD26 activity inhibition- and gene deletion-mediated defect in HSPC mobilization and transendothelial migration. (A) Mass spectrometric validation of DPP4-dependent proteolysis of NPY to NPY₃₋₃₆. Purified NPY (1 μg) was treated with DPP4 (0.1 μg) overnight. (B) NPY levels in BM SECs and in BMEF from G-CSF-treated WT mice (mean ± SEM; n = 5 mice/group). Positive gates for NPY expression were based on FMO (green). (C) Transendothelial migration of LSK cells across BMECs treated with G-CSF, G-CSF plus diprotin A, or G-CSF plus diprotin A with NPY₃₋₃₆ (mean ± SEM; n = 2 experiments; 3 mice/experiment). (D) Transendothelial migration of CD34⁺ cells across HUVECs treated with G-CSF, G-CSF plus diprotin A, or G-CSF plus diprotin A with NPY₃₋₃₆ (mean ± SEM; n = 3 experiment; using 3 individual CB samples). (E and F) Blood CFU-Cell (CFU-C) and SLAM LSK cell counts in WT mice treated with G-CSF and in CD26^{-/-} mice treated G-CSF, G-CSF plus NPY, or G-CSF plus NPY₃₋₃₆ (mean ± SEM; n = 5 mice/group). (G) Donor chimerism in PB at 6 months in Boyl mice competitively transplanted using equal volumes of PB from mice (C57BL/6) treated with G-CSF, G-CSF plus diprotin A, G-CSF plus diprotin A with NPY, or G-CSF plus NPY₃₋₃₆ in combination with 200,000 BM cells from Boyl mice (left) and tri-lineage reconstitution of donor cells (right) (mean ± SEM; n = 5 mice/group). (H) CFU-C mobilization in WT and NPY^{-/-} mice treated with G-CSF, G-CSF plus diprotin A, or G-CSF plus diprotin A with NPY₃₋₃₆ (mean ± SEM; n = 5 mice/group). (I) CFU-C mobilization in WT mice treated with G-CSF alone or with selective NPYR2 (BIIE 0246) or NPYR5 (CGP 71683 hydrochloride) inhibitors (mean ± SEM; n = 4 mice/group). *P < 0.05 compared with vehicle and †P < 0.05 compared with G-CSF-treated WT mice, by Student's t test (B) or 1-way ANOVA with Sidak's multiple comparisons test (C-I).

assays, the number of WT and CD26^{-/-} Lin⁻ (Figure 4B, left) and LSK (Figure 4B, right) cells migrating across monolayers of mouse BMECs toward SDF-1 was enhanced by G-CSF and blocked by diprotin A. This enhancement was equivalent for both WT and CD26^{-/-} HSPCs, further indicating that HSPC-intrinsic CD26 is not involved in transendothelial migration. Enhanced transendothelial migration was not specific to SDF-1 but was also seen to the chemoattractant sphingosine-1-phosphate (SP1), which was also blocked by diprotin A (Figure 4C). These results demonstrate that G-CSF increases EC CD26 expression and activity and that CD26 activity enhances HSPC transendothelial migration.

CD26-cleaved NPY regulates HSPC transendothelial migration and mobilization. Since CD26 cleaves the N-terminus of effector proteins and our data indicated that cleavage of SDF-1 was not a mechanism through which CD26 affects hematopoietic trafficking, we hypothesized that an alternative protein containing an N-terminal CD26 cleavage site is mechanistically involved. A systematic search of protein sequence databases for proteins containing putative CD26 recognition sites intriguingly identified the neurotransmitter NPY (26), a ligand with cognate receptors on monocytes, osteoblasts, stromal cells, and ECs and that has been shown to regulate immune cell and bone homeostasis (27–30). In addition, recent studies suggest a role for NPY in the regulation of BM niche components and HSPC trafficking (31, 32). To test the potential role of CD26-cleaved NPY in regulating HSPC trafficking in response to G-CSF, we first validated by mass spectrometry that CD26 cleaved NPY to the expected truncated NPY₃₋₃₆ form (Figure 5A). We next found an increased frequency of NPY⁺ BM SECs after G-CSF treatment (Figure 5B, left) and elevated NPY protein levels in the BMEF (Figure 5B, right). Although NPY is also expressed in other niche cells including macrophages, nestin⁺ MSCs, and CD45⁺Ter119⁺CD31⁻ nonendothelial stromal cells, expression of NPY in these cell populations was not affected by G-CSF treatment (Supplemental Figure 4A). These results suggest that the dynamically regulated NPY within the BM after G-CSF treatment is most likely of EC origin.

To further examine the role of CD26-truncated NPY in endothelial activity, we performed HSPC transendothelial migration assays. As we previously observed, treatment of mouse BMECs with G-CSF enhanced transendothelial migration of HSPCs, and this enhancement could be blocked by diprotin A treatment. However, addition of the truncated NPY₃₋₃₆ restored enhanced transendothelial migration in G-CSF plus diprotin A-treated culture (Figure 5C). Similarly, treatment of HUVEC monolayers with G-CSF increased the transendothelial migration of cord blood (CB) CD34⁺ cells that was blocked by diprotin A and restored by truncated NPY₃₋₃₆ but not full-length NPY (Figure 5D). These data indicate that truncated NPY₃₋₃₆ signaling on ECs enhances HSPC transendothelial migration and identified a potential mechanism to explain the enhanced mobilization seen in the presence of CD26 activity.

Full-length NPY interacts with several G protein-coupled receptors, preferentially binding to the NPY1 receptor, whereas NPY₃₋₃₆ preferentially binds to the Y2 and Y5 NPY receptors (33). Flow cytometric analysis indicated that BM SECs expressed Y1, Y2, and Y5 receptors (Supplemental Figure 4B). If truncated NPY is responsible for optimal HSPC mobilization in response to

G-CSF, then the reduced mobilization phenotype seen in CD26^{-/-} mice or in mice treated with diprotin A should be reversed by treatment of mice with the truncated NPY₃₋₃₆. Administration of NPY₃₋₃₆ to CD26^{-/-} mice restored the attenuated colony-forming cell (CFC) (Figure 5E) and SLAM LSK cell (Figure 5F) mobilization response to G-CSF to the level seen in WT mice. Similarly, coadministration of NPY₃₋₃₆ and G-CSF reversed the attenuation of CFC mobilization (Supplemental Figure 5A) and transplantable long-term repopulating HSCs (Figure 5G) by diprotin A. Administration of NPY or truncated NPY alone had no effect on basal HSPC trafficking (Supplemental Figure 5B). Since NPY₃₋₃₆ was able to overcome the attenuated mobilization response to G-CSF seen in genetic and pharmacological models lacking CD26 activity, we hypothesized that mice lacking NPY should also show an attenuated response to mobilization by G-CSF and that blockade of CD26 activity in NPY-deficient mice should not further attenuate mobilization. Consistent with a recent report (31), mice lacking NPY demonstrated attenuated mobilization to G-CSF (Figure 5H). In addition, we found that this was not affected by blockade of CD26 activity with diprotin A. Reduced mobilization of HSPCs in NPY-KO mice following G-CSF treatment did not result from impaired HSPC expansion, since the numbers of marrow SLAM LSK cells in WT mice and NPY-KO mice were equivalent at baseline and after G-CSF treatment (Supplemental Figure 5C). Most important, NPY₃₋₃₆ administration restored the G-CSF mobilization response of NPY-KO mice to the levels observed in WT mice (Figure 5H), identical to the response seen in CD26^{-/-} mice. As the truncated NPY signals through the NPY2 and NPY5 receptors, blocking signaling through one or more of those receptors would be expected to mimic a lack of CD26 activity. In WT mice, coadministration of selective NPY2 (BIIE 0246) and NPY5 (CGP 71683) receptor antagonists reduced HSPC mobilization by G-CSF to a degree similar to that seen in CD26^{-/-} and NPY-KO mice (Figure 5I).

NPY₃₋₃₆ increases vascular permeability. Since NPY receptors have been previously shown to differentially regulate vascular tone (34), and since our in vitro data showed that truncated NPY₃₋₃₆ enhances transendothelial migration and our in vivo data indicated that NPY₃₋₃₆, via the NPY2 and NPY5 receptors, enhances HSPC mobilization, we investigated whether CD26-dependent proteolytic cleavage of NPY affects vascular permeability, thereby facilitating HSPC migration and mobilization into the PB. To start, we again used confluent BMEC monolayers in vitro. Treatment of EC cultures with G-CSF resulted in increased dextran-FITC permeability (Figure 6A) that was blocked by diprotin A and restored by NPY₃₋₃₆ but not full-length NPY. We observed identical effects using HUVECs (data not shown). While BMEC monolayers are useful as a model for transendothelial migration and permeability, we sought to validate this effect in the intact hematopoietic niche in vivo by measuring vascular permeability across BM endothelium using intravital imaging. In vivo, 150-kDa dextran permeability was significantly (Figure 6B) higher in mice that were treated with G-CSF compared with that seen in the vehicle control mice (Figure 6B). This increased vascular permeability after G-CSF was substantially reduced in mice cotreated with diprotin A but was restored by coadministration of NPY₃₋₃₆ (Figure 6C). To further support our findings of NPY₃₋₃₆

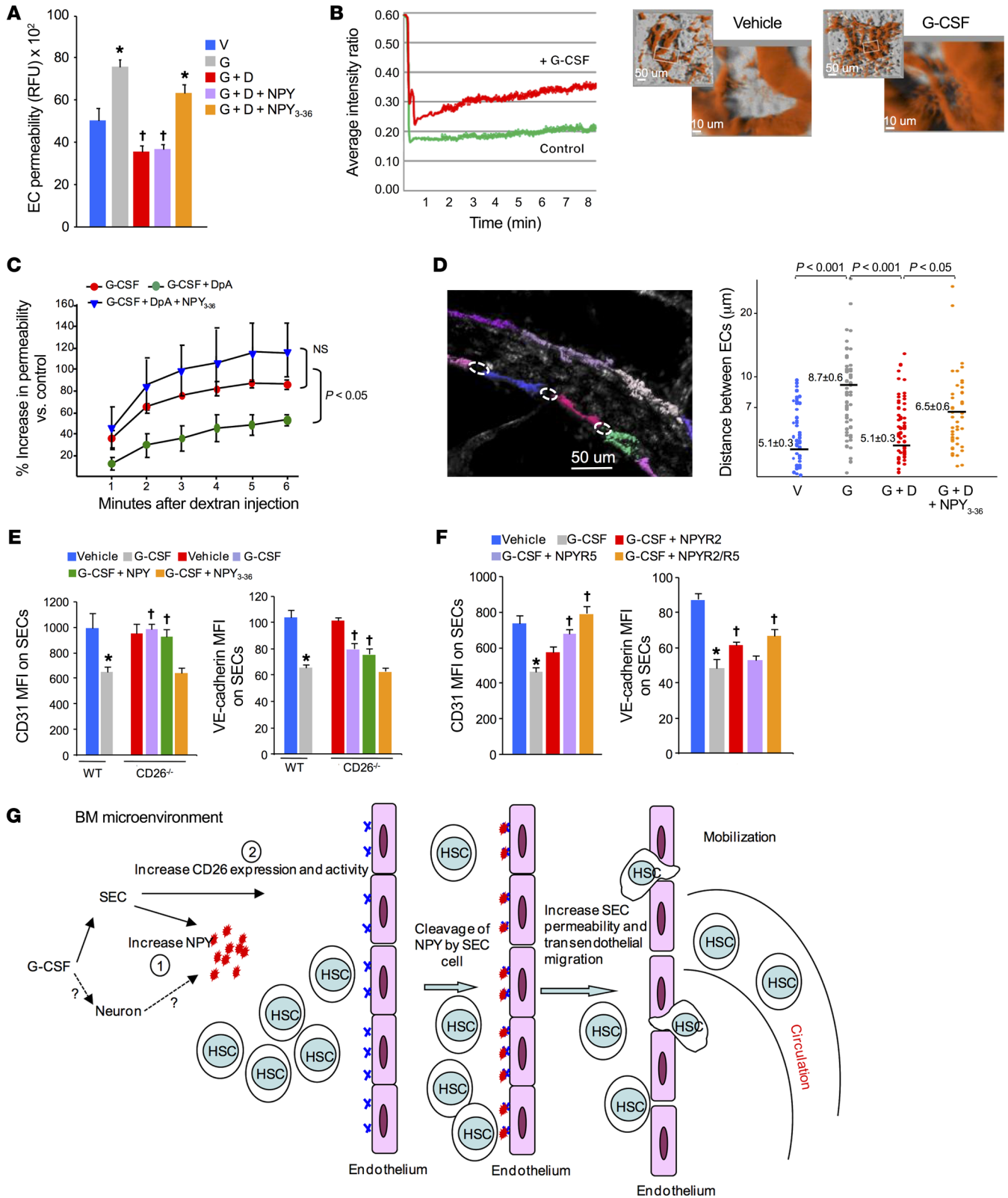


Figure 6. NPY₃₋₃₆ reduces EC contact and increases permeability. (A)

Measurement of dextran-FITC permeability across confluent BMEC monolayers treated with G-CSF, G-CSF plus diprotin A, G-CSF plus diprotin A with NPY, or G-CSF plus diprotin A with NPY₃₋₃₆ for 24 hours (mean ± SEM; $n = 2$ experiments, 3 mice/experiment). $P \leq 0.05$ compared with vehicle treated mice and $^{\dagger}P \leq 0.05$ compared with G-CSF-treated mice, by 1-way ANOVA with Sidak's multiple comparisons test. **(B and C)** Measurement of vascular permeability in calvarial BM from mice treated with G-CSF, G-CSF plus diprotin A, or G-CSF plus diprotin A with NPY₃₋₃₆. **(B)** Representative intravital 2-photon images of calvarial BM from vehicle- or G-CSF-treated mice and representative average fluorescence intensity ratio for each vessel/interstitial space in vehicle- and G-CSF-treated mice. **(C)** Average increase in vascular permeability compared with vehicle control (mean ± SEM; $n = 4-6$ mice/group, each assayed individually). 1-way ANOVA with Sidak's multiple comparisons test was used to determine the P values and $^*P < 0.05$ compared with G-CSF treated mice was considered significant. **(D)** Intravital 2-photon image analysis of the distance between individual ECs in isolectin B4-labeled evaluable vessels in BM from mice treated with G-CSF, G-CSF plus diprotin A, or G-CSF plus diprotin A with NPY₃₋₃₆ (mean ± SEM; $n = 4$ mice/group; ≥ 15 fields/mouse). 1-way ANOVA with Sidak's multiple comparisons test was used to determine the P value and $P \leq 0.05$ was considered significant. **(E)** CD31 and VE-cadherin expression on BM SECs from WT mice treated with G-CSF and from CD26^{-/-} mice treated with G-CSF, G-CSF plus NPY, or G-CSF plus NPY₃₋₃₆ (mean ± SEM; $n = 4$ mice/group). **(F)** CD31 and VE-cadherin expression on BM SECs from mice treated with G-CSF alone or in combination with selective NPYR2 (BIIE 0246) or NPYR5 (CGP 71683 hydrochloride) antagonists (mean ± SEM; $n = 4$ mice/group). **(E and F)** $^*P < 0.05$ compared with vehicle treated WT mice and $^{\dagger}P \leq 0.05$ compared with G-CSF-treated WT mice, by 1-way ANOVA with Sidak's multiple comparisons test. **(G)** Model of NPY₃₋₃₆-regulated vascular permeability and HSPC egress from BM. In response to G-CSF, CD26 expression and activity are enhanced on BMECs, which converts NPY into NPY₃₋₃₆ and shifts NPY signaling on ECs from the NPY1 receptors that enforce vascular integrity to the NPY2 and NPY5 receptors that downregulate CD31 and VE-cadherin along endothelial gap junctions, resulting in increased vascular permeability and enhanced HSPC transendothelial egress.

effects on permeability, we measured the distances between EC junctions. Intravital 2-photon image examination of isolectin B4-labeled BM vessels showed a significantly increased gap distance between ECs after G-CSF treatment (Figure 6D) that was substantially blocked by cotreatment with diprotin A. Consistent with the permeability assays, NPY₃₋₃₆ administration reversed the blocking effect of diprotin A and increased the gap distance to an extent similar to that observed with G-CSF alone. In addition, the BM vessel diameter in G-CSF-treated mice was significantly higher compared with that in vehicle controls (Supplemental Figure 5D). These results demonstrate that truncated NPY₃₋₃₆ increases the distance between ECs, enhancing vascular permeability and subsequent transendothelial migration and mobilization of HSPCs.

NPY regulates EC interactions. Vascular permeability is regulated by a coordinated opening and closing of EC junctions that is primarily mediated by VE-cadherin and PECAM-1 (CD31) (35, 36). Consistent with increased vascular permeability and transendothelial migration, G-CSF treatment of HUVEC monolayers resulted in significantly reduced expression of CD31 and VE-cadherin along cell-cell contacts (Supplemental Figure 6A). Blockade of CD26 activity with diprotin A prevented reduced CD31 and VE-cadherin expression along cell junctions, whereas cotreatment with truncated NPY₃₋₃₆, but not full-length NPY, restored the loss of CD31 and VE-cadherin expression along cell-cell contacts to an

extent similar to that seen with G-CSF alone. We observed similar effects on primary BM SECs in vivo (Figure 6E). Basal CD31 and VE-cadherin levels were similar in WT and CD26^{-/-} mice; however, following G-CSF administration, we observed substantially decreased CD31 and VE-cadherin expression on BM SECs from WT mice, but only moderately reduced expression on BM SECs from CD26^{-/-} mice. Coadministration of NPY₃₋₃₆, but not full-length NPY, with G-CSF resulted in a reduction of CD31 and VE-cadherin levels in CD26^{-/-} mice equal to that seen with G-CSF treatment in WT mice. Reduced VE-cadherin expression on EC junctions after G-CSF treatment was due to its internalization (Supplemental Figure 6B). CD26 inhibition prevented VE-cadherin internalization, whereas truncated NPY₃₋₃₆ restored internalization to the levels detected with G-CSF alone. VE-cadherin and CD31 mRNA expression was not altered during the G-CSF mobilization regimen (Supplemental Figure 6C). We found that expression of EC Robo 4, which has previously been linked to vascular permeability (37), was not altered in response to G-CSF, with or without diprotin A (Supplemental Figure 6D).

Blockade of NPY2 and NPY5 receptor signaling with receptor-specific antagonists during G-CSF mobilization substantially increased CD31 and VE-cadherin expression on BM sinusoidal endothelium, with the combination of NPY2 and NPY5 antagonists being more effective than either antagonist alone (Figure 6F). These results indicate that truncated NPY₃₋₃₆ acts through both receptors to downregulate VE-cadherin and CD31, increasing EC spacing and vascular permeability and facilitating HSPC egress to the PB.

Our results suggest that ECs act as active gatekeepers regulating HSPC egress from BM and that the enzymatic cleavage of NPY by CD26 can regulate this gatekeeper function. To determine whether this role of ECs as gatekeepers for HSPC egress was specific to G-CSF or more broadly applicable to inducers of HSPC trafficking, we used the CXCR4 antagonist AMD3100, which mobilizes HSPC independently of CD26 activity. Treatment of mice with truncated NPY₃₋₃₆, but not intact NPY, enhanced AMD3100-induced CFU-GM (Supplemental Figure 6E) and the SLAM LSK cell mobilization (Supplemental Figure 6F) that were associated with reduced expression of VE-cadherin on BMECs (Supplemental Figure 6G). These studies indicate that regulation of vascular permeability is a common feature associated with HSPC BM egress and mobilization.

Discussion

Numerous earlier studies have described roles for BMECs in the hematopoietic niche as regulators of homeostasis and hematopoietic recovery after stress. Here, we demonstrate for the first time to our knowledge that the BM endothelium actively regulates trafficking of HSPCs. Here, we show that control of hematopoietic trafficking occurs through a NPY/EC axis that is differentially regulated via enzymatic cleavage by CD26. In response to G-CSF, BMECs increase CD26 activity, resulting in the conversion of NPY into its truncated form NPY₃₋₃₆. This truncated ligand shifts the NPY signaling on ECs from NPY1 receptors that enforce and maintain vascular integrity to the NPY2 and NPY5 receptors that downregulate CD31 and VE-cadherin along endothelial gap junctions. The result of this signaling shift is increased vascular per-

meability and enhanced HSPC transendothelial egress. NPY signaling on ECs acts as the gatekeeper for HSPCs, and enzymatic cleavage by CD26 determines whether the gateway for exit from the marrow is open or closed.

Enzymatic N-terminal cleavage by CD26 can modulate the bioavailability and activity of growth factors, cytokines, and chemokines known to regulate hematopoiesis (7, 8, 38). The SDF-1/CXCR4 axis enforces HSPC retention within the BM (15, 19). The facts that SDF-1 can be truncated by CD26 (8, 12) and SDF-1 protein levels are reduced in G-CSF-treated mice (13, 18, 19) led to an assumption that the reduced HSPC trafficking in CD26^{-/-} mice was the result of higher levels of intact BM SDF-1. Contrary to this assumption, we found an identical reduction of active BM SDF-1 in both WT and CD26-KO mice treated with G-CSF, despite the fact that mobilization was impaired in the KO mice. In addition, the proportioned reduction in SDF-1 transcripts and protein following G-CSF treatment (17, 18) suggests that SDF-1 expression during G-CSF mobilization is predominantly regulated at the transcriptional level and not by posttranslational modification. Therefore, alteration of SDF-1 activity by CD26 does not appear to be a critical mechanism governing HSPC trafficking in response to G-CSF.

In most cases, enzymatic cleavage by CD26 leads to protein inactivation, as is the case with SDF-1 (39, 40), or to decreased activity, such as what occurs with the hematopoietic factors GM-CSF, IL-3, and EPO (7). In the case of GM-CSF, CD26 truncation results in enhanced receptor binding, but also inhibition of the higher-order receptor oligomerization needed for maximal activity. Intact NPY has high binding affinity for the Y1 receptor on ECs that enforces vasoconstriction (30, 34), whereas the enzymatically cleaved NPY₃₋₃₆ preferentially binds to the Y2 and Y5 receptors and has been shown to enhance leukocyte trafficking (28). In contrast to many of the proteins that CD26 is capable of enzymatically altering, the conversion of NPY by CD26 changes the specific receptors through which the ligand functions, fundamentally altering the resultant response. We demonstrate here that cleavage of NPY by CD26 is a key regulator of induced HSPC exit from the marrow space and that the “open door” signal comes from NPY2 and NPY5 signaling. This specific paradigm that truncation alters which receptor a ligand binds to is evident in our studies exploring NPY and the regulation of vascular permeability and clearly points to the need for further exploration of CD26 and other posttranslational enzymatic activities in the alteration of biologic responses during dynamic scenarios such as stress or disease.

Recently, it was reported that NPY might regulate HSPC mobilization by enhancing MMP-9 activity via signaling through the Y1 receptor (31). However, we found similar levels of MMP-9 in mice treated with G-CSF or G-CSF plus diproton A. The similar levels of MMP-9 after CD26 activity inhibition, despite reduced vascular permeability and HSPC mobilization, indicate that the role of CD26 regulation of NPY and mobilization is MMP-9 independent and suggest the potential involvement of parallel mechanisms by which NPY can modulate G-CSF-induced mobilization. Moreover, although neutrophil-derived MMP-9 is implicated in HSPC mobilization (41, 42), our chimeric studies do not support a direct role for neutrophils or their proteolytic enzymes in the enhancement of vascular permeability by NPY, although we cannot rule out the possibility of an indirect effect of

stroma-derived cleaved NPY on neutrophils that affects vascular permeability. While we cannot rule out pleiotropic effects of NPY on other cell types, particularly considering the differences in full-length versus truncated signaling that we demonstrate here, our results show that the enzymatically controlled vascular gateway is specifically opened by truncated NPY signaling via NPY2 and NPY5 receptors. Inhibition or genetic deletion of *Cd26* exclusively suppresses G-CSF-induced enhancement in vascular permeability, without affecting the other stromal components and retention factors we explored. The ability of exogenous truncated NPY₃₋₃₆ to increase vascular permeability to the level seen with G-CSF treatment strongly supports the idea that this CD26/NPY signaling axis regulates G-CSF-induced HSPC mobilization by acting as a vascular gatekeeper. As there are currently no available mouse strains with endothelium-specific KO of CD26, NPY2, or NPY5, we cannot absolutely rule out the contribution of other stromal components in the CD26/NPY axis that may be involved in HSPC egress in response to G-CSF. However, G-CSF increases CD26 activity exclusively on ECs and not on other stromal cell populations, supporting our conclusion that this signaling axis acts on ECs and plays a predominant role in vascular permeability.

To expand beyond our G-CSF model system and explore the regulatory role of CD26 and NPY in an independent hematopoietic trafficking model, we used the CXCR4 antagonist AMD3100. Our finding that truncated, but not intact, NPY enhanced mobilization by AMD3100 and was associated with decreased EC VE-cadherin expression suggests that BM SECs act as common active gateways for HSPC egress. Cleavage components of the complement cascade also induce EC permeability (43) and HSPC mobilization (44, 45). It may be interesting in the future to explore whether the combination of complement peptides with truncated NPY can further increase mobilization. In general, the possibility of controlling vascular permeability and integrity has several therapeutic applications beyond the collection of HSPCs for transplantation. An uncontrolled and lasting increase in permeability that is not balanced by the reabsorption of lymphatic fluid causes edema, which in turn increases ischemic tissue injury in conditions such as stroke or myocardial infarction. In addition, vascular permeability in tumors facilitates tumor cell penetration into the vessels and metastatic dissemination. Vascular barrier dysfunction is also a central feature of endotoxin shock, and the combination of LPS and cytokines increases NPY expression and CD26 activity on human ECs *in vitro* (46). Our *in vivo* mouse models exploring the CD26/NPY axis support the possibility that CD26-truncated NPY results in enhanced vascular permeability as a result of endotoxin exposure. In this context, preliminary studies suggest that inhibition of CD26 activity or administration of full-length NPY prevents the suppression of endothelial VE-cadherin expression normally observed in LPS-treated mice and that therapeutic targeting of NPY signaling has the potential to control vascular permeability in sepsis and is worth further exploration.

In summary, our data define a signaling axis, whereby enzymatic cleavage of NPY switches the receptor signaling of the ligand and reduces vascular integrity, resulting in hematopoietic egress from the marrow space (Figure 6G). These studies

point to ECs as gatekeepers of HSPC trafficking in and out of BM and enzymatic regulation of NPY by CD26 as the open or close signal. The responsiveness of NPY receptors to soluble ligands and synthetic antagonists *in vivo* makes them excellent pharmacological targets for regulating HSPC trafficking in homeostatic and stress conditions and may have broad utility beyond hematopoiesis, including control of inflammatory reactions and augmentation of the vascular permeability associated with bacterial infection and dissemination.

Methods

Mice and cell lines. C57BL/6, *Npy*-KO (129 129S1/SvImJ background), and 129S1/SvImJ mice were purchased from The Jackson Laboratory. *Cd26*^{-/-} mice (C57BL/6 background) were provided by Hal Broxmeyer (Indiana University, Indianapolis, Indiana, USA). Experiments were performed using 9- to 12-week-old mice. Murine BMECs were purchased from Cell Biologics, and HUVECs were purchased from ATCC. ATCC uses short tandem repeat (STR) profiling for cell line authentication and tests for mycoplasma in their cell products; cells were used from freshly thawed vials. No further authentication or mycoplasma testing was performed.

Reagents. Human G-CSF was purchased from Amgen. Diprotin A was obtained from Calbiochem. Antibodies against c-Kit (clone 2B8), Sca-1 (clone D7), lineage (clone 17A2/RB6-8C5/RA3-6B2/Ter-119/M1/70), CD48 (clone HM48-1), and CD31 (clone MEC13.3) were purchased from BioLegend. Antibodies against CD150 (clone mShad150), VEGFR3 (clone AFL4), and VE-cadherin (clone eBioBV13) were obtained from BD Biosciences. Anti-CD26 (clone 155202), anti-Robo4 (clone 274904), anti-nestin (clone 307501), and anti-leptin receptor (Ala20Gly839) antibodies were purchased from R&D Systems. Antibody against SDF-1 (clone 2B11) was purchased from Thermo Fisher Scientific. Mouse Lineage Depletion Kits (catalog 130-090-858) were purchased from Miltenyi Biotec.

HSPC mobilization and isolation of cells. PB stem cell (PBSC) mobilization was induced by s.c. administration of 1 μ g G-CSF/mouse twice daily for 4 days, as we described previously (42). Mice were treated with diprotin A (Ile-Pro-Ile; Calbiochem) (10 μ g/day) to inhibit CD26 enzyme activity. For some experiments, mice received NPY₁₋₃₆ or NPY₃₋₃₆ (1 μ g/day) (MilliporeSigma) for the last 2 days of G-CSF treatment. Mice were sacrificed 16 hours after the last G-CSF treatment. Complete blood counts (CBCs) were determined using a Hemavet 950F hematology analyzer (Drew Scientific).

Hematopoietic and nonhematopoietic BM cell isolation. BM cells were harvested by flushing femurs with cold α -MEM (Lonza Biologics) containing 2% FBS (Hyclone). To isolate bone-associated cells, femurs and tibiae were crushed using a mortar and pestle and incubated with 0.25% collagenase type 1 (Invitrogen, Thermo Fisher Scientific) for 1 hour at 37°C. Cells were collected after filtering through 40- μ m filters.

Lineage depletion and flow cytometric analysis. Mobilized blood mononuclear cells (MNCs) or whole BM cells were treated with FcR Block (BD Biosciences) and Lin⁻ cells enriched by incubation with anti-CD11b, anti-Ly6G, anti-TCR, anti-CD45R, and anti-TER119, followed by negative selection with a biotin selection system (Miltenyi Biotec). Lin⁻ cells were stained with anti-Sca-1, anti-c-Kit, anti-CD150, anti-CD48, and anti-CD26 for detection of CD26 expression on phenotypically defined HSPC populations. After staining, cells were fixed with 1% paraformaldehyde (PFA) and analyzed by flow cytometry. For

intracellular SDF-1 detection in leptin receptor⁺ mesenchymal stromal cells and nestin⁺ MSCs, BM cells were first stained with anti-CD45, anti-Ter119, anti-CD31, and anti-leptin receptor antibodies followed by fixation and permeabilization and then stained with anti-nestin and anti-SDF-1 antibodies.

Progenitor cell functional assays. Mobilized PB (25 μ m) was lysed with RBC lysis buffer (eBioscience) and cultured in methylcellulose medium containing growth factors as described previously (42). The plates were incubated in a humidified atmosphere of 5% CO₂ and 5% O₂ for 7 days, and CFCs were enumerated microscopically.

BM and PB transplantation. Chimeric mice were generated by transplanting 1 \times 10⁶ whole BM cells from WT or CD26^{-/-} mice into lethally irradiated (1,150 cGy split dose) congenic WT or CD26^{-/-} recipients. Two months after transplantation, mice were treated with G-CSF for 4 days, and HSPC mobilization was determined by FACS immunophenotyping and CFC assay. To evaluate long-term HSC mobilization with G-CSF, G-CSF plus diprotin A, or G-CSF plus diprotin A with NPY₃₋₃₆, 50 μ l RBC lysed blood samples from mobilized mice (CD45.2⁺) plus 200,000 competitive whole BM cells from untreated CD45.1⁺ mice (in a total volume of 200 μ l) were transplanted into lethally irradiated CD45.1⁺ recipient mice. PB chimerism and multilineage reconstitution were assessed 16 weeks after transplantation.

ELISA. BMEF was obtained by flushing 1 femur with 1 ml ice-cold PBS followed by centrifugation at 400 g for 3 minutes. Cell-free supernatants were used to measure soluble, nonmembrane-bound SDF-1, stem cell factor (SCF), osteoprotegerin (OPG), and NPY by ELISA (R&D Systems).

DPP4 enzyme activity measurement. Murine BM cells were digested with collagenase type 1 for 30 minutes, stained for cell-surface markers (HSPCs, osteolineage cells, or ECs) and evaluated by flow cytometry for DPP4 enzyme activity using H-Gly-Pro-AMC. In brief, after cell-surface staining, BM cells were resuspended in 50 μ l supplemented Iscove's modified Dulbecco's medium (IMDM) and incubated with 5 μ l of a 0.3-mM solution of AMC-conjugated dipeptides (Gly-Pro) for 10 minutes at 37°C. At the end of the incubation period, enzymatic activity was stopped by placing the tubes in 4°C, and the DPP4 activity of LSK, osteolineage, and EC gated cell populations was measured.

Mass spectroscopy and receptor affinity assay for intact and CD26-cleaved SDF-1. Recombinant mouse (rm) CXCL12/SDF-1 α (10 μ g/50 μ l) (R&D Systems) was incubated with mouse DPP4 (R&D Systems) overnight at 37°C, and cleavage products were analyzed by MALDI-TOF mass spectroscopy at the Mass Spectrometry Facility of Indiana University. Binding of SDF-1 to Jurkat T cell CXCR4 was determined by flow cytometry. Intact or DPP4-treated rmSDF-1 cells were incubated with Jurkat cells (50,000 cells in 100 μ l 10% RPMI) for 90 minutes at 4°C. Cells were washed twice and incubated with biotin-conjugated anti-SDF-1 (clone BAF310; R&D Systems) for 45 minutes at 4°C, followed by streptavidin-PE-conjugated secondary antibody (BD Biosciences) for 30 minutes at 4°C. To quantitate SDF-1 in BMEF, femurs and tibiae were flushed with PBS and cell-free supernatants passed through 3-kDa molecular weight cutoff filters. Concentrated BMEFs were incubated with Jurkat cells, and SDF-1 binding was quantitated by flow cytometry. To detect membrane-bound SDF-1, BM cells were stained with cell-surface marker-specific antibodies and anti-SDF-1 antibody and analyzed by flow cytometry.

Transendothelial migration. Mouse BMECs or HUVECs were placed into the upper chambers of Transwell inserts (5- μ m) (Corning) and cultured for 2 days to achieve confluent monolayers. Conflu-

ent monolayers were washed and treated with G-CSF (100 ng/ml), alone or with diprotin A (100 ng/ml) and/or NPY₁₋₃₆ or NPY₃₋₃₆ (100 ng/ml) for 24 hours. Following incubation, the treated monolayers were washed twice and overlaid with WT or CD26^{-/-} Lin⁻ mouse BM cells or CD34⁺ CB cells. LSK cell migration to rmSDF-1 (100 ng/ml) or S1P (100 ng/ml) and CD34⁺ cell migration to rhSDF-1 (100 ng/ml) was quantitated by flow cytometry after 4 hours. The percentage of migrated cells was calculated by dividing the total number of cells that migrated to the lower well by the cell input multiplied by 100. LSK cell migration was determined by comparison of the proportion of LSK cells in the input and migrated cell populations.

Immunofluorescence and IHC. For the quantitation of VE-cadherin and CD31 expression at cell junctions, HUVEC monolayers were fixed with 4% paraformaldehyde for 10 minutes at 4°C. Monolayers were washed twice and incubated with FITC anti-VE-cadherin and biotin anti-CD31 antibodies (BioLegend) for 1 hour at 4°C, followed by streptavidin-Texas red antibody (Alpha Diagnostic Inc). Samples were examined under a Leica DM 2500 fluorescence microscope outfitted with a QImaging MicroPublisher camera (W. Nuhsbaum). Immunohistochemical analysis was performed on decalcified paraffin-embedded tissue sections. Rabbit polyclonal antibodies against VEGFR-3 and SDF-1 α were from Abcam. Secondary anti-rabbit antibodies were purchased from VECTOR Laboratories. HRP-rat IgG2 isotype was used as a primary antibody negative control for VEGFR3 and SDF-1 at 1:50.

Permeability assays and measurement of distance between ECs. BM vascular permeability was assessed via intravital 2-photon imaging of niches in mouse calvariae. Mice were anesthetized, and 150-kDa TRITC-conjugated dextran (TdB Consultancy; 100 μ l of 20 mg/ml solution per animal) was injected into a catheterized jugular vein. To monitor dextran extravasation, calvariae were exposed, and a time series acquisition (XYT) of a chosen BM area was performed at a scan rate of 2 μ s/pixel, with no averaging, and a frame size of 512 \times 256 (1.048 \times 1.048 μ m pixel size). All images were acquired with an Olympus FV1000 confocal system (Olympus America), custom modified for multiphoton imaging at the Indiana Center for Biological Microscopy (Indianapolis, Indiana, USA) and equipped with a Mai Tai HP Laser (Spectra-Physics) and GaAsP photo multiplier tubes (Hamamatsu). Image analysis was performed using Metamorph image analysis software, version 7.7 (Molecular Devices). To monitor tracer dynamics, the average fluorescence intensity (AFI) was calculated in regions of the blood vessel and adjacent interstitial space for 3 vessels in a field and frame by frame. An AFI ratio for each vessel/interstitial space was calculated and plotted.

To measure the distance between ECs, mice were injected i.v. with Alexa Fluor 488-conjugated isolectin IB4 (Invitrogen, Thermo Fisher Scientific; 100 μ g/mouse). Twenty minutes after injection, the mice were anesthetized, and images were acquired as described above. The Z-stack images were analyzed using the Imaris software package, version 8.1 (Bitplane). Surpass view was used to display stacks as maximum-intensity or alpha-blend projections. Single ECs were segmented using the Surface Segmentation module, and then the Surface-Surface XTension was used to calculate the shortest distances between surfaces of adjacent cells. These studies were performed at the ICBM Imaging Facility of the Indiana University School of Medicine.

For in vitro permeability assays, mouse BMEC monolayers were cultured on the membranes of the upper chambers of Transwell inserts (5- μ m pore size) and treated with G-CSF, G-CSF plus diprotin

A, or G-CSF plus diprotin A with NPY₃₋₃₆ for 24 hours. After treatment, 4,000-kDa molecular weight FITC-dextran was added on top of the EC monolayers, allowing the fluorescent molecules to pass through for 30 minutes. The extent of BMEC monolayer permeability was determined using fluorimetry to measure the relative fluorescence units (RFU) of FITC-dextran in the bottom chamber.

VE-cadherin internalization. HUVEC monolayers were grown on chambered coverglass. Anti-VE-cadherin antibody (MilliporeSigma; clone BV-6) was incubated with cell monolayers at 4°C on ice for 30 minutes in EBM-2 media (Lonza). Unbound antibody was removed by rinsing cells in ice-cold PBS. Cells were cultured in EBM-2 medium and treated with G-CSF, G-CSF plus diprotin A, or G-CSF plus diprotin A with NPY₃₋₃₆ for 16 hours at 37°C. At the end of the incubation period, monolayers were fixed with PFA (4% for 30 min), and images were acquired with an Olympus FV1000 confocal system. Z-stack images were analyzed using the Imaris software package, version 8.1 (Bitplane). Imaris' Surpass view was used to display stacks as maximum-intensity or alpha-blend projections. Cells were segmented on the basis of cytoplasmic staining using the Surface Segmentation module. The total cadherin signal (represented as the volume) was obtained using the SPOT Segmentation module, and the intracellular fraction of cadherin was calculated by applying a mask of cytoplasmic staining over the cadherin channel.

Statistics. All WT and KO mice were age and sex matched, and cages were randomly assigned to the treatment groups. The number of animals used in the experiments was estimated to give sufficient power (>90%) on the basis of the effect sizes observed in our preliminary data. Grubbs' test was used to identify the outliers, and no animals were excluded from the analysis. In vivo and in vitro processing steps were not blinded, but imaging readouts were analyzed in a blinded manner. All the statistical analyses were performed using Excel or GraphPad Prism 7 (GraphPad Software). Statistical significance for binary comparisons was assessed by 2-tailed Student's *t* test, and data were normally distributed with sufficiently equivalent variances. For comparison of more than 2 groups, ANOVA with Sidak's multiple comparisons test was used. All data are reported as the mean \pm SEM. A *P* value of 0.05 or less was considered significant.

Study approval. These studies were performed according to the recommendations of the NIH's *Guide for the Care and Use of Laboratory Animals* (National Academies Press, 2011). The IACUC of the Indiana University School of Medicine reviewed and approved the study protocols.

Author contributions

PS designed the study, executed the experiments, analyzed and interpreted data, and wrote the manuscript. JH participated in designing the experiments and wrote the manuscript. KSM and TAG performed histologic analyses and assisted with the corresponding study designs. MRS analyzed histology. MMK and NC performed and analyzed 2-photon live imaging for vascular permeability. HL and JS performed and analyzed quantitative reverse transcription PCR (qRT-PCR) data. LMP supervised the study, designed and executed experiments, analyzed data, and wrote the manuscript.

Acknowledgments

This work was supported by NIH grants HL096305, CA182947, and AG046246 (to LMP) and CA143057 and LA069158 (to TAG

and KSM). Flow cytometry was performed at the Flow Cytometry Resource Facility of the Indiana University (IU) Melvin and Bren Simon Cancer Center (National Cancer Institute [NCI] grant P30 CA082709). Flow cytometry and live animal imaging were also supported by a Center of Excellence Grant in Molecular Hematology (PO1 DK090948).

Address correspondence to: Louis M. Pelus or Pratibha Singh, Department of Microbiology and Immunology, Indiana University School of Medicine, 950 West Walnut Street, Indianapolis, Indiana 46202, USA. Phone: 317.274.7565; Email: lpelus@iupui.edu (L.M. Pelus). Phone: 317.274.9944; Email: pratsing@iupui.edu (P. Singh).

- Morrison SJ, Scadden DT. The bone marrow niche for haematopoietic stem cells. *Nature*. 2014;505(7483):327–334.
- Hoggatt J, Scadden DT. The stem cell niche: tissue physiology at a single cell level. *J Clin Invest*. 2012;122(9):3029–3034.
- Hoggatt J, Pelus LM. Mobilization of hematopoietic stem cells from the bone marrow niche to the blood compartment. *Stem Cell Res Ther*. 2011;2(2):13.
- Hoggatt J, Speth JM, Pelus LM. Concise review: Sowing the seeds of a fruitful harvest: hematopoietic stem cell mobilization. *Stem Cells*. 2013;31(12):2599–2606.
- Christopherson KW, Cooper S, Hangoc G, Broxmeyer HE. CD26 is essential for normal G-CSF-induced progenitor cell mobilization as determined by CD26^{-/-} mice. *Exp Hematol*. 2003;31(11):1126–1134.
- Christopherson KW, Cooper S, Broxmeyer HE. Cell surface peptidase CD26/DPP4 mediates G-CSF mobilization of mouse progenitor cells. *Blood*. 2003;101(12):4680–4686.
- Broxmeyer HE, et al. Dipeptidylpeptidase 4 negatively regulates colony-stimulating factor activity and stress hematopoiesis. *Nat Med*. 2012;18(12):1786–1796.
- Lambeir AM, et al. Kinetic investigation of chemokine truncation by CD26/dipeptidyl peptidase IV reveals a striking selectivity within the chemokine family. *J Biol Chem*. 2001;276(32):29839–29845.
- Mentlein R, Roos T. Proteases involved in the metabolism of angiotensin II, bradykinin, calcitonin gene-related peptide (CGRP), and neuropeptide Y by vascular smooth muscle cells. *Peptides*. 1996;17(4):709–720.
- Ou X, O'Leary HA, Broxmeyer HE. Implications of DPP4 modification of proteins that regulate stem/progenitor and more mature cell types. *Blood*. 2013;122(2):161–169.
- Van Damme J, et al. The role of CD26/DPP IV in chemokine processing. *Chem Immunol*. 1999;72:42–56.
- Ohtsuki T, et al. Negative regulation of the anti-human immunodeficiency virus and chemotactic activity of human stromal cell-derived factor 1alpha by CD26/dipeptidyl peptidase IV. *FEBS Lett*. 1998;431(2):236–240.
- Kollet O, et al. Osteoclasts degrade endosteal components and promote mobilization of hematopoietic progenitor cells. *Nat Med*. 2006;12(6):657–664.
- Dar A, et al. Chemokine receptor CXCR4-dependent internalization and resecretion of functional chemokine SDF-1 by bone marrow endothelial and stromal cells. *Nat Immunol*. 2005;6(10):1038–1046.
- Lévesque JP, Hendy J, Takamatsu Y, Simmons PJ, Bendall LJ. Disruption of the CXCR4/CXCL12 chemotactic interaction during hematopoietic stem cell mobilization induced by G-CSF or cyclophosphamide. *J Clin Invest*. 2003;111(2):187–196.
- Christopherson KW, Hangoc G, Broxmeyer HE. Cell surface peptidase CD26/dipeptidylpeptidase IV regulates CXCL12/stromal cell-derived factor-1 alpha-mediated chemotaxis of human cord blood CD34⁺ progenitor cells. *J Immunol*. 2002;169(12):7000–7008.
- Méndez-Ferrer S, et al. Mesenchymal and hematopoietic stem cells form a unique bone marrow niche. *Nature*. 2010;466(7308):829–834.
- Semerad CL, et al. G-CSF potently inhibits osteoblast activity and CXCL12 mRNA expression in the bone marrow. *Blood*. 2005;106(9):3020–3027.
- Petit I, et al. G-CSF induces stem cell mobilization by decreasing bone marrow SDF-1 and up-regulating CXCR4. *Nat Immunol*. 2002;3(7):687–694.
- Nakamura Y, et al. Isolation and characterization of endosteal niche cell populations that regulate hematopoietic stem cells. *Blood*. 2010;116(9):1422–1432.
- Zhou BO, Yue R, Murphy MM, Peyer JG, Morrison SJ. Leptin-receptor-expressing mesenchymal stromal cells represent the main source of bone formed by adult bone marrow. *Cell Stem Cell*. 2014;15(2):154–168.
- Crump MP, et al. Solution structure and basis for functional activity of stromal cell-derived factor-1; dissociation of CXCR4 activation from binding and inhibition of HIV-1. *EMBO J*. 1997;16(23):6996–7007.
- Butler JM, et al. Endothelial cells are essential for the self-renewal and repopulation of Notch-dependent hematopoietic stem cells. *Cell Stem Cell*. 2010;6(3):251–264.
- Ding L, Saunders TL, Enikolopov G, Morrison SJ. Endothelial and perivascular cells maintain haematopoietic stem cells. *Nature*. 2012;481(7382):457–462.
- Chen JY, et al. Hoxb5 marks long-term hematopoietic stem cells and reveals a homogenous perivascular niche. *Nature*. 2016;530(7589):223–227.
- Frerker N, et al. Neuropeptide Y (NPY) cleaving enzymes: structural and functional homologues of dipeptidyl peptidase 4. *Peptides*. 2007;28(2):257–268.
- Straub RH, et al. Neuropeptide Y cotransmission with norepinephrine in the sympathetic nerve-macrophage interplay. *J Neurochem*. 2000;75(6):2464–2471.
- Bedoui S, et al. NPY modulates epinephrine-induced leukocytosis via Y-1 and Y-5 receptor activation in vivo: sympathetic co-transmission during leukocyte mobilization. *J Neuroimmunol*. 2002;132(1-2):25–33.
- Ekblad E, Edvinsson L, Wahlestedt C, Uddman R, Håkanson R, Sundler F. Neuropeptide Y co-exists and co-operates with noradrenaline in perivascular nerve fibers. *Regul Pept*. 1984;8(3):225–235.
- Zukowska-Grojec Z, et al. Neuropeptide Y: a novel angiogenic factor from the sympathetic nerves and endothelium. *Circ Res*. 1998;83(2):187–195.
- Park MH, et al. Neuropeptide Y induces hematopoietic stem/progenitor cell mobilization by regulating matrix metalloproteinase-9 activity through Y1 receptor in osteoblasts. *Stem Cells*. 2016;34(8):2145–2156.
- Park MH, et al. Neuropeptide Y regulates the hematopoietic stem cell microenvironment and prevents nerve injury in the bone marrow. *EMBO J*. 2015;34(12):1648–1660.
- Mentlein R, Dahms P, Grandt D, Krüger R. Proteolytic processing of neuropeptide Y and peptide YY by dipeptidyl peptidase IV. *Regul Pept*. 1993;49(2):133–144.
- Li L, Demuth HU, Zukowska Z. Dipeptidyl peptidase IV: a molecular switch of vascular actions of neuropeptide Y. *Adv Exp Med Biol*. 2006;575:135–140.
- Gavard J, Gutkind JS. VEGF controls endothelial-cell permeability by promoting the beta-arrestin-dependent endocytosis of VE-cadherin. *Nat Cell Biol*. 2006;8(11):1223–1234.
- Privratsky JR, Paddock CM, Florey O, Newman DK, Muller WA, Newman PJ. Relative contribution of PECAM-1 adhesion and signaling to the maintenance of vascular integrity. *J Cell Sci*. 2011;124(Pt 9):1477–1485.
- Smith-Berdan S, Nguyen A, Hong MA, Forsberg EC. ROBO4-mediated vascular integrity regulates the directionality of hematopoietic stem cell trafficking. *Stem Cell Reports*. 2015;4(2):255–268.
- Mentlein R. Dipeptidyl-peptidase IV (CD26) – role in the inactivation of regulatory peptides. *Regul Pept*. 1999;85(1):9–24.
- Proost P, et al. Processing by CD26/dipeptidyl-peptidase IV reduces the chemotactic and anti-HIV-1 activity of stromal-cell-derived factor-1alpha. *FEBS Lett*. 1998;432(1-2):73–76.
- Sadir R, Imberty A, Baleux F, Lortat-Jacob H. Heparan sulfate/heparin oligosaccharides protect stromal cell-derived factor-1 (SDF-1)/CXCL12 against proteolysis induced by CD26/dipeptidyl peptidase IV. *J Biol Chem*. 2004;279(42):43854–43860.
- Heissig B, et al. Recruitment of stem and progenitor cells from the bone marrow niche requires MMP-9 mediated release of kit-ligand. *Cell*.

- 2002;109(5):625–637.
42. Pelus LM, Bian H, King AG, Fukuda S. Neutrophil-derived MMP-9 mediates synergistic mobilization of hematopoietic stem and progenitor cells by the combination of G-CSF and the chemokines GRObeta/CXCL2 and GRObetaT/CXCL2delta4. *Blood*. 2004;103(1):110–119.
43. Williams TJ. Vascular permeability changes induced by complement-derived peptides. *Agents Actions*. 1983;13(5-6):451–455.
44. Lee HM, et al. Impaired mobilization of hematopoietic stem/progenitor cells in C5-deficient mice supports the pivotal involvement of innate immunity in this process and reveals novel mobilization effects of granulocytes. *Leukemia*. 2009;23(11):2052–2062.
45. Jalili A, et al. Fifth complement cascade protein (C5) cleavage fragments disrupt the SDF-1/CXCR4 axis: further evidence that innate immunity orchestrates the mobilization of hematopoietic stem/progenitor cells. *Exp Hematol*. 2010;38(4):321–332.
46. Silva AP, Cavadas C, Baisse-Agushi B, Spertini O, Brunner HR, Grouzmann E. NPY, NPY receptors, and DPP IV activity are modulated by LPS, TNF-alpha and IFN-gamma in HUVEC. *Regul Pept*. 2003;116(1-3):71–79.